MODELING AND SIMULATION OF FINNED TUBE EVAPORATOR MODEL DURING FROST CONDITIONS

Abstract. *The behavior of air forced evaporator is quite relevant for refrigerated products industry. A good performance of such heat exchanger provides lower energy consumptions and better level of conservation of products.*

Regarding the operation of air forced evaporators during frosting conditions, the prediction of the degradation of the capacity of such equipments is quite important, especially when related to the conservation of products.

The modeling of those heat exchangers presents a challenge. Firstly, due to the evaluation of heat transfer coefficients and pressure drop levels in the refrigerant side due to the occurrence of two-phase flow combined with the different refrigerant circuitries as well as tube geometries (internal fins, elliptical cross section, etc.). Secondly, the air side heat and mass transfer coefficients and the pressure drop level have their own challenges regarding the evaluation of the amount of formed frost during the air cooling process and the impacts on air flow and fin efficiency.

This paper proposes a modeling and simulation of air forced evaporators during frost formation and a comparison with experimental data taken from an experimental bench specifically for this purpose. The comparison shows a good agreement with the experimental data and provides insight for improving the operational procedures of such evaporators.

Keywords*: refrigeration, air forced evaporator, modeling, simulation, frost.*

1. INTRODUCTION

The use of refrigeration started as early as 1875 (Thévenot, 1979) and evolved through several stages till our days. During this evolution, several issues were studied such as the thermal modeling and design optimization of the evaporator. Some of the aspects related to such studies are temperature control and frost formation. The latter one influences several aspects of conservation of products, especially temperature control and energy conservation of the refrigerated chamber.

The modeling of an air forced evaporator has several challenges due to its complexity related to air and refrigerant convection heat transfer where two-phase flow patterns and frost formation are present. Regarding specifically to frost formation, its occurrence promotes the heat transfer degradation which results in capacity reduction of the evaporator, requiring a defrosting process to restore this capacity. This frosting/defrosting cycle imposes a severe variation on the temperature of the refrigerated chamber, which can result in the degradation of the product.

The main purpose of this paper is to present a model for simulating an air forced evaporator under frosting conditions and evaluate the parameters that influence the thermal behavior of such heat exchanger on such conditions.

2. Literature review

Storey & Jacobi (1999) analyzed the frost formation in air cooled evaporators with vortex generators for heat transfer enhancement in refrigeration applications. Storey & Jacobi evaluated, in an experimental bench, the frost growth for different conditions (surface temperature: -23 to -6 °C; Reynolds number: 300 to 2500; relative humidity: 30 to 70%). They concluded that frost thickness was independent of the Reynolds number and proportional to the square root of the frost formation time. Storey & Jacobi verified that the presence of vortex generators promotes a 7.2% increase in the frost layer thickness compared to the smooth surfaces. The vortex generators also produced changes in the frost formation processes that modify frost physical properties, particularly by reducing its thermal resistance. Therefore, Storey & Jacobi concluded that the vortex generators, besides enhancing the heat transfer, can reduce the frost thermal resistance, promoting an increase in the overall heat transfer coefficient. Storey & Jacobi did not produce any tests to evaluate the air side pressure drop.

Deng et al. (2003) analyzed the influence of frost formation in the performance of finned tube evaporators with 6, 8 and 10 mm fin spacing. For the testes performed by the authors, parameters such as the evaporation temperature, the thickness of the frost layer and air velocity were modified. A logarithmic temperature and enthalpy difference was employed to evaluate the performance of the air forced evaporators. Based on the experimental data, the authors evaluated that, due to the increase on the growth of the frost layer:

- the overall heat transfer coefficient increases in the beginning of the frost formation process and then decreases;

- the smaller the fin spacing is, the quicker the overall heat transfer coefficient decreases. This decrease can achieve reductions of 50% comparing to the coefficient without frost formation. These results show that bigger fin spacing is more suitable when there is a heat transfer process with frost formation.

Yan et al. (2003) evaluated experimental results related to the performance of heat exchangers with smooth fins and frost formation. The variation of parameters such as air relative humidity, air dry bulb temperature, air mass flow, refrigerant temperature, fin height and number of rows were done. The performance of such heat exchangers was evaluated based on the following parameters: heat transfer rate, overall heat transfer coefficient and air pressure drop. Regarding the thickness of the frost layer, Yan et al. observe that:

- there is a decrease on the heat transfer rate and on the overall heat transfer due to an increase on the air mass flow, the dry bulb temperature and relative humidity;
- there is a decrease on the heat transfer rate and on the overall heat transfer due to an increase on the air pressure drop;
- because of an increase in the refrigerant temperature and fin height an increase in the overall heat transfer is experienced;
- a negligible variation on the heat transfer rate and in the air pressure drop is evaluated due to an increase in the refrigerant temperature and fin height;

Hoffenbecker et. al (2005) presented a model for an air forced evaporator defrosting using refrigerant superheated vapor known as hot gas defrost. Their model used parameters such air dry bulb temperature and relative humidity, evaporator geometry, frost layer thickness and density and hot gas temperature in the evaporator inlet section. The model discretizes the evaporator and calculates energy and mass balances in order to characterize the heat and mass transfer processes during the defrost operation. The results show a small uncertainty compared to the experimental data found in the open literature. The results indicate that the optimum hot gas temperature is dependent of the accumulated mass and the density of the frost.

Jheea et al. (2002) analyzed the effect of surface roughness on frost formation and on the defrost process for finned tube heat exchangers. The authors verified that hydrophilic surfaces affect more the frost formation. On the other hand, hydrophobic surfaces turn the defrost process more efficient and faster.

Seker et al. (2004a e b) presented a model and an experimental validation of the performance of a finned tube evaporator with frost formation. The transient semi empirical model is developed for household freezer conditions, where specific constitutive equations for molecular diffusion and heat transfer were used. The main hypotheses regarding frost formation were:

- frost is distributed uniformly along the evaporator;
- average physical properties for the frost layer are applied;
- the frost thermal conductivity is assumed density dependent only.

The comparison between experimental data and the model shows that the model can reproduce the tendency of the evaporator’s thermal performance regarding the overall heat transfer and air pressure drop but with an average uncertainty of 20 to 25%.

3. Experimental bench

The experimental bench used to evaluate the data for this paper is shown in Fig. 01. For that bench the following parameters and their uncertainties are presented in Tab. 1. In this bench, it was possible to control the parameters shown in Tab. 1 by adjusting the control valve, the heaters input and the compressor speed. These adjustments were made manually which implied in several hours to achieve proper test condition. In order to regulate the relative humidity, a humidifier produced water vapor and it was controlled by the relative humidity sensor in the inlet section of the evaporator. In order to control and acquire the data, a dedicated data acquisition is used.

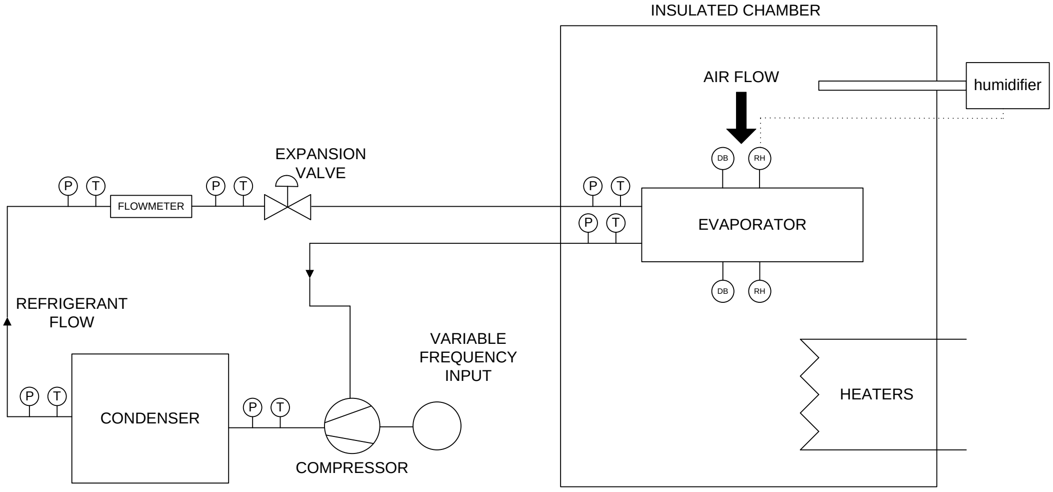

Figure 1. Simplified experimental bench

Table 1. Experimental test bench uncertainty.

Parameter	Uncertainty
Refrigerant temperature	±0,3ºC
Air dry bulb temperature	±0,5ºC
Refrigerant pressure	±10kPa
Refrigerant mass flow	0,1% of the measurement

The tests were divided into two sets: one where the air forced evaporator was tested without frost formation and one with frost formation. This division was made in order to separate the effects of the frost in the performance of the evaporators. For each set, the parameters and their range are shown in Tab. 2. For each test, by evaluating an energy balance for the evaporator, the heat transfer rate was calculated and its uncertainty was evaluated as 8.3%, using the values shown in Tab. 1. Four different evaporators were tested with geometrical characteristics shown on Tab. 3. The tube was made of copper and the fins were made of aluminum for all the evaporators.

Table 2. Parameters range for the tests.

Parameter	Variation
Refrigerant evaporation temperature [°C]	-5, -10, -15, -20, -25
Air dry bulb temperature [°C]	(*)
Fin spacing [mm]	4,23(6 fins/pol) and 6,35 (4 fins/pol)
Inlet air relative humidity [%]	70 to 90

(*)Obs.: The air dry bulb temperature was controlled and kept at 6ºC above the refrigerant evaporation temperature.

Table 3. Geometrical characteristics.

	Evaporators			
Parameter	#1	#2	#3	#4
Fin spacing [mm]	4,23(6 fins/inch)	6,35 (4 fins/inch)	4,23(6 fins/inch)	6,35 (4 fins/inch)
Length [mm]	325	635	325	635
Tube to Tube distance [mm]	20	20	20	20
Row distance [mm]	20	20	20	20
Internal diameter [mm]	12	12	12	12
Rows [-]	4	4	4	4
Fin height [mm]	20	20	20	20
Fin thickness [mm]	0,18	0,18	0,18	0,18

The test procedure follows the ones described on a ASHRAE standard (ASHRAE, 2001). Those procedures specify that the experimental bench parameters should be adjust until ±0.6ºC temperature variation is achieved. After reaching a steady state condition, a set of 30 minutes of data was taken by the data acquisition system. The frost was prevented from being formed by turning on an electrical defrost system. Similar procedures were reproduced on the test where frost was allowed to be formed where the defrost system was turned off and measurements of each parameter was done continuously in 01 minute intervals until the face area of the evaporator was completely blocked by the frost formed during the test. An example of an evaporator heat transfer curve for one test is shown in Fig.2.

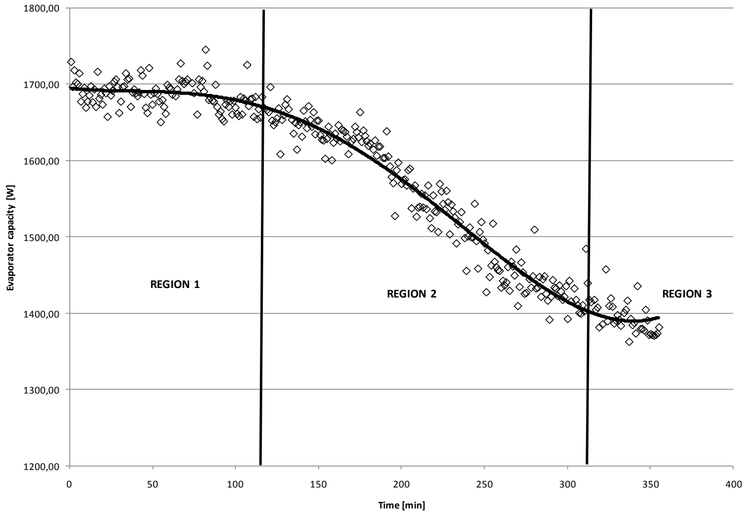

Figure 2. Evaporator heat transfer rate curve during frost formation test.

One can notice that in Fig. 2 there are three regions: region 1 where the evaporator is frost free, region 2 where the frost is formed and region 3 where the evaporator is completely blocked by the formed frost. The criteria to determine where region 2 starts and finishes takes into account the average heat transfer rate determined in regions 1 and 3. The instant where region 2 starts corresponds to the time when the heat transfer rate is 8.3% lower than the average heat transfer rate evaluated in region 1. Similarly, the instant when region 2 finishes is when the heat transfer rate is 8.3% higher than average heat transfer rate in region 3. The time period related to region 2 is the time necessary to have the evaporator completely blocked and it can be used as a parameter to evaluate the process of frost formation. Therefore this parameter, named in this paper as frosting time, was plotted against the parameters range shown in Tab. 2.

One can notice on Fig. 3 that the frosting time decreases while the evaporation temperature decreases. Similar behavior is noticed when the frosting time is plotted against the fin spacing where for a smaller fin spacing the frosting time decreases (see Fig. 4). Finally, the frosting time is plotted against the relative humidity and an increase of frosting time is verified for an increase of the relative humidity (see Fig. 5).

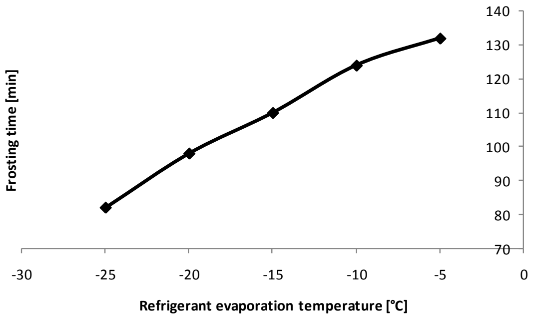

Figure 3. Frosting time against evaporation refrigerant temperature

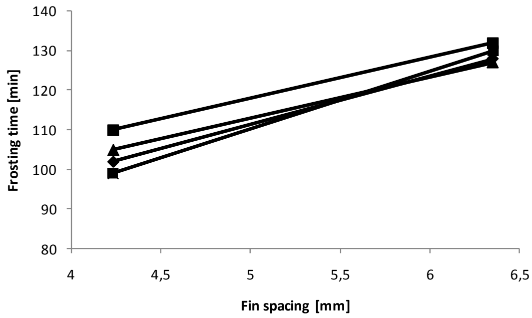

Figure 4. Frosting time against fin spacing

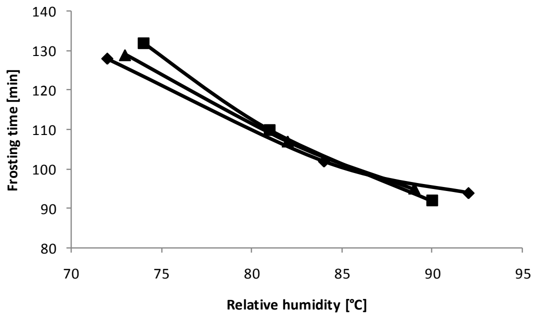

Figure 5. Frosting time against relative humidity.

4. Semi-empirical model

Based on the tests made previously, a semi-empirical model is proposed where the evaporator length is divided in 20 sections and for each section an energy balance is performed in each section with the following hypotheses:

- the air and refrigerant pressure drop are negligible;
- the quality varies linearly;
- the frost is distributed uniformly along each section.

Therefore, the energy balance in each section in the refrigerant side can be calculated as:

$$\dot{q}_{refrigerant} = \dot{m}_{refrigerant}\left(h_{outlet,ref} - h_{inlet,ref}\right) \tag{1}$$

Where: $\dot{q}_{refrigerant}$ = refrigerant side heat transfer rate [W];
$\dot{m}_{refrigerant}$ = refrigerant mass flow rate [kg/s];
$h_{outlet,ref}$ = outlet section refrigerant enthalpy [J/kg]
$h_{inlet,ref}$ = inlet section refrigerant enthalpy [J/kg]

$$\dot{q}_{air} = \dot{m}_{air}\left(h_{outlet,air} - h_{inlet,air}\right) \tag{2}$$

Where: $\dot{q}_{air}$= air side total heat transfer rate [W];
$\dot{m}_{air}$ = air mass flow rate [kg/s];
$h_{outlet,air}$ = outlet section air enthalpy [J/kg]
$h_{inlet,air}$ = inlet section enthalpy [J/kg]

The air side energy balance can be divided in three portions, i.e.:

$$\dot{q}_{air} = \dot{q}_{sensible} + \dot{q}_{condensation} + \dot{q}_{frost} \tag{3}$$

Where: $\dot{q}_{air}$= air side total heat transfer rate [W];
$\dot{q}_{sensible}$ = air side sensible heat transfer rate [W];
$\dot{q}_{condensation}$ = heat transfer rate for water vapor condensation [W];
$\dot{q}_{frost}$ = heat transfer rate for frost formation [W];

The sensible portion can be calculated as:

$$\dot{q}_{sensible} = UA\left(T_{air} - T_{refrigerant}\right) \tag{4}$$

Where: $\dot{q}_{sensible}$ = air side sensible heat transfer rate [W];
U = overall heat transfer coefficient [W/m^2.K];
A = external heat transfer area [m^2];
T_{air} = average air dry bulb temperature in each section [°C];
$T_{refrigerant}$ = average refrigerant temperature in each section[°C];

The external area *A* and the overall heat transfer coefficient *U* varied along the tests due to the increase in the frost layer thickness and Eq. 3 is used for *U* evaluation.

$$U = \frac{1}{\frac{1}{h_{refrigerant}} + \frac{e_{frost}}{k_{frost}} + \frac{1}{h_{air}\eta_{fin}}} \quad (5)$$

Where: $h_{refrigerant}$ = refrigerant side convection heat transfer [W/m^2.K];
h_{air} = air side convection heat transfer [W/m^2.K];
e_{frost} = frost layer thickness [m];
k_{frost} = frost layer thermal conductivity [W/m.K];
η_{fin}= fin effectiveness [-];

Eqs. 6 to 12 (Oskarsson et al,1990) were found more suitable to calculate the refrigerant side convection heat transfer.

$$h_{refrigerant} = h_{mix} * (1-\alpha) + h_{vapor} * \alpha \quad (6)$$

Where:

$$h_{mix} = 0{,}0009 * \frac{k_l}{D_i} * \left[Re^2 * K_f\right]^{0,5} \quad (7)$$

$$Re = \frac{G * D_i}{\mu_l} \quad (8)$$

$$K_f = \frac{(x_{outlet} - x_{inlet})h_{lv}}{Lg} \quad (9)$$

k_l = liquid refrigerant thermal conductivity [W/m.K];
D_i = tube internal diameter [m];
μ_l = refrigerant dynamic viscosity [N.s/m^2];
G = mass flux [kg/s.m^2];
x_{oulet} and x_{inlet} = outlet and inlet refrigerant quality, respectively [-];
h_{lv} = difference between the refrigerant saturated vapor and saturated liquid enthalpy [J/kg];
L = section length [m];
g = gravity [m/s^2];

$$h_{vapor} = 0{,}0108 * Cp_v^{1/3} k_v^{2/3} \mu_v^{-2/3} Re_v \quad (10)$$

Cp_v = refrigerant vapor specific heat [J/kg.K];
k_v = refrigerant vapor thermal conductivity [W/m.K];
μ_v = refrigerant vapor dynamic viscosity [N.s/m^2];

$$Re_v = \left(\frac{G * D_i}{\mu_v}\right)^{-0.1375} \quad (11)$$

$$\bar{x} = \frac{(x_{outlet} - x_{inlet})}{2} \quad (12)$$

Eqs. 13 to 19 were used for the air side convection coefficient evaluation. These equations are valid to smooth finned tubes evaporators with 1 to 4 rows (Mcquiston et al, 1981).

$$h_{air} = \frac{j Cp_{air} G_{max}}{Pr^{2/3}} \quad (13)$$

Where:

$$j = 0.2675P + 1.325x10^{-6} \quad (14)$$

$$P = Re_D^{-0.4} \left(\frac{A_o}{A_t}\right)^{-0.15} \quad (15)$$

$$\frac{A_o}{A_t} = \frac{4}{\pi} \frac{S_L}{D_h} \frac{S_R}{D} \quad (16)$$

$$\sigma = \frac{A_{min}}{A_f} \quad (17)$$

$$Re_D = \frac{G_{max} D}{\mu_{air}} \quad (18)$$

$$D_h = \frac{4 A_{min} S_L}{A_o} \quad (19)$$

A_o = total air side surface area = (A_t + A_f) [m^2]
A_t = bare tube outside area [m^2]
A_f = fin surface area [m^2]
A_{min} = minimum free flow area [m^2]

S_L = distance between rows [m]
S_R = distance between tubes [m]
D_h = hydraulic tube diameter for the minimum free flow area [m]
D = outside tube diameter [m]
G_{max} = air mass flux for the minimum free flow area [kg/s.m^2]
Re_D = Reynolds number [-]
Cp_{air} = air specific heat evaluated for the average air temperature [J/kg.K]
μ_{air} = air dynamic viscosity evaluated for the average air temperature [N.s/m^2]

The fin effectiveness was calculated as shown in Eqs. 20 to 26 (Incropera et al., 2007) where the main assumptions were that a weighted thermal conductivity were calculated based on the fin material and frost thickness. Therefore, this parameter varies during the frost formation process. Senshu et al (1990) proposed a model to evaluate the frost thermal conductivity and density that is shown in Eqs. 24 and 25 and it proved to be suitable for this study.

$$\eta_{fin} = \frac{\tanh(mL_c)}{mL_c} \quad (20)$$

Where:

L_c = L+ t/2 = fin perimeter [m] (21)
t_{fin} = fin thickness [m]

$$m = \sqrt{\frac{2h_{air}}{k_{eq}t_{eq}}} \quad (22)$$

$t_{eq} = t_{fin} + 2t_{frost}$ = equivalent fin thickness [m] (23)

$$k_{eq} = \frac{t_{eq}}{\frac{t_{fin}}{k_{fin}} + 2\frac{t_{frost}}{k_{frost}}} \quad (24)$$

k_{fin} = fin thermal conductivity [W/m.K]

$k_{frost} = 0.02422 + 0.0000011797 * \rho_{frost}^2 + 0.007241 * \rho_{frost}$=frost thermal conductivity [W/m.K] (25)

$\rho_{frost} = 650 * e^{0.177*T_s}$= frost density [kg/m^3] (26)

T_s = frost surface temperature [K]

Equations 1 to 26 were solved for each section for a given time step by imposing the refrigerant and air mass flow and the inlet refrigerant and air temperature and pressure, obtained from the experimental data. The frost mass was also calculated and the frost layer thickness was evaluated based on the uniform distribution hypothesis. This procedure was done until the evaporator free area is totally filled with frost. The outputs parameters of the model were the outlet evaporator temperature and the capacity for every time and they are compared with the experimental data. A comparison of the model results with the experimental data for the evaporator capacity for a frost free condition is shown in Fig 6.

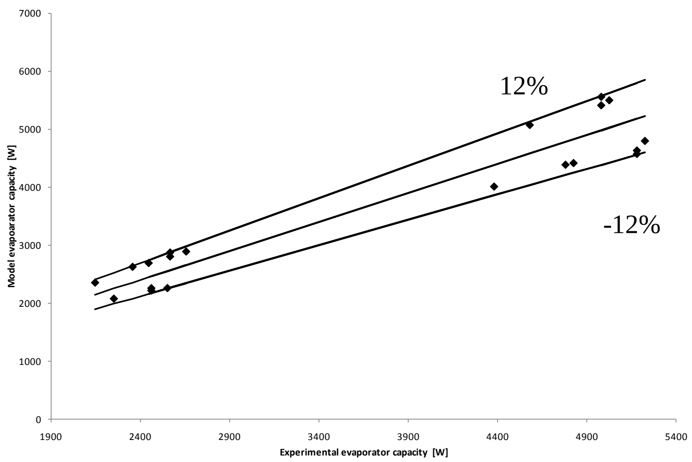

Figure 6. Comparison between experimental and model evaporator capacity.

One can see that the variation of the evaporator capacity between the experimental data and the model results is between ±12% for 90% of the experimental data, which can be considered a fair result. It also can be seen that there were two separate groups of data: the right group is related to the smaller heat exchangers (#1 and 2) and the left group is for the bigger heat exchangers (#3 and 4). An uncertainty of ±1.2ºC was found when comparing the experimental and the model evaporator outlet section temperature. This high uncertainty can be explained by an increase of the refrigerant temperature in the final sections where the void fraction is near 1. An improvement on the heat transfer model should be revised and implemented for that region.

The model was then used to evaluate the frost formation time. The experimental and model frost formation time is compared. The average uncertainty for the frost formation time is 18%. The model always underestimated the frost formation time comparing to the experimental data. This can be explained by the initial hypothesis of having an uniform frost distribution that led to higher velocity of the face area blockage than the actual heat exchangers experienced. Therefore, detailed experiments should be carried on in order to better evaluate the frost distribution in the heat exchanger and the model should be improved.

5. Final considerations

A comparison between experimental data and a numerical model was made for the heat transfer rate of finned tube heat exchangers under frosting conditions. The average uncertainty for the frost free conditions was ±12% and an overestimation of 1.2ºC was evaluated for the refrigerant temperature of the outlet section of the evaporator. The frosting formation time was compared between the experimental data and the numerical model for the frosting conditions. There was 18% underestimation of such parameter which indicates that improvements should be done in the numerical model and more detailed experimental tests should be carried on. These results indicated that improvements should be done in order to reduce the difference between the experimental and model values.

The use of such model can become a useful tool for a better prediction on how frost formation affects the evaporator performance. This can be applied to optimize the defrost control system of air forced evaporator for low temperatures applications.

6. Acknowledgements

The authors would like to acknowledge the support of FAPESP for supporting this research.

7. References

ASHRAE. 2001. Standard 25-2001 – Methods of Testing Forced Convection and Natural Convection Air Coolers for Refrigeration, ASHRAE, 25 pages.

Deng, D.; Xu, L.; Xu, S. 2003. Experimental investigation on the performance of air cooler under frosting conditions. Applied Thermal Engineering, Vol. 23, pp. 905-912.

Hoffenbecker, N.; Klein, S.A.; Reindl; D.T. 2005. Hot gas defrost model development and validation. International Journal of Refrigeration, Vol. 28, pp. 605-615.

Incropera, F. P.; DeWitt, D. P.; Bergman, T. L.; Lavine, A. S. .2007. Fundamentals of Heat and Mass Transfer, 6th edition, 643 pages.

Jheea, S.; Leeb, K.; Kimb, W. 2002. Effect of surface treatments on the frosting/defrosting behavior of a fin-tube heat exchanger. International Journal of Refrigeration, Vol. 25, pp. 1047-1053.

McQuiston, F. C. 1981. Finned Tube Heat Exchangers: state of art for the air side. ASHRAE Transactions, Vol. 87, Part 1.

Seker, D.; Karatas, H.; Egrican, N. 2004a. Frost formation on fin-and-tube heat exchangers. Part I—Modeling of frost formation on fin-and-tube heat exchangers. International Journal of Refrigeration, Vol. 27, pp. 367-374.

Seker, D.; Karatas, H.; Egrican, N. 2004b. Frost formation on fin-and-tube heat exchangers. Part II—Experimental investigation of frost formation on fin- and- tube heat exchangers. International Journal of Refrigeration, Vol. 27, pp. 375-377.

Senshu, T.; Yasuda, H.; Oguni, K. Ishibane, K. 1990. Heat pump under frosting conditions: Part I, Heat and Mass Transfer on Cross-finned Tube Heat Exchangers under Frosting Conditions ASHRAE Transactions, Vol. 96, Part I, pp. 324-329.

Storey, B.D.; Jacobi, A.M. The effect of streamwise vortices on the frost growth rate in developing laminar channel flows. International Journal of Heat and Mass Transfer, Vol. 42, pp. 3787-3802, 1999.

Thévenot, R. 1979. A History of Refrigeration, International Institute of Refrigeration, 476 pages.

Yan, W.; Li, H.; Wu, Y.; Lin, J.; Chang, W. Performance of finned tube heat exchangers operating under frosting conditions. International Journal of Heat and Mass Transfer, Vol. 46, pp. 871-877, 2003.

7. RESPONSIBILITY NOTICE